Soft Matter

EMERGING AREA

View Article Online
View Journal | View Issue

CrossMark click for updates

Cite this: *Soft Matter*, 2015, 11, 8897

Femtosecond laser controlled wettability of solid surfaces

Jiale Yong, Feng Chen,* Qing Yang* and Xun Hou

Received 26th August 2015,
Accepted 22nd September 2015

DOI: 10.1039/c5sm02153g

www.rsc.org/softmatter

Femtosecond laser microfabrication is emerging as a hot tool for controlling the wettability of solid surfaces. This paper introduces four typical aspects of femtosecond laser induced special wettability: superhydrophobicity, underwater superoleophobicity, anisotropic wettability, and smart wettability. The static properties are characterized by the contact angle measurement, while the dynamic features are investigated by the sliding behavior of a liquid droplet. Using different materials and machining methods results in different rough microstructures, patterns, and even chemistry on the solid substrates. So, various beautiful wettabilities can be realized because wettability is mainly dependent on the surface topography and chemical composition. The distinctions of the underlying formation mechanism of these wettabilities are also described in detail.

Open Access Article. Published on 22 September 2015. Downloaded on 2/12/2026 6:34:48 AM. This article is licensed under a Creative Commons Attribution 3.0 Unported Licence.

1. Introduction

Wettability plays a very important role in the survival of creatures and in our daily life.[1–10] Recently, much attention has been paid to fabrication of special wettable surfaces due to their significance in basic research studies, practical applications, and bionics.[11–20] Four typical aspects of wettability are widely studied by researchers, namely superhydrophobicity, superoleophobicity, anisotropic wettability, and smart wettability. A surface with a water contact angle (WCA) larger than 150° is generally defined as a superhydrophobic surface.[21–24] Superhydrophobicity is the earliest one studied. If the liquid object is another very popular liquid in daily life: oil, the oil-repellent surface is called a superoleophobic surface. Following the same principle of superhydrophobicity, superoleophobicity is the same as an oil droplet showing an oil contact angle (OCA) higher than 150°.[25–28] In nature, a water droplet on a rice leaf has different WCA values, as well as sliding angles (SAs), along two vertical directions.[29–31] This anisotropic property is caused by the ordered arrangement of the rough micro-papillas on rice leaves. The static characteristic (anisotropic wetting) and the dynamic feature (anisotropic sliding) are two

Key Laboratory of Photonics Technology for Information of Shaanxi Province & State Key Laboratory for Manufacturing System Engineering, School of Electronics & Information Engineering, Xi'an Jiaotong University, Xi'an, 710049, P. R. China. E-mail: chenfeng@mail.xjtu.edu.cn, yangqing@mail.xjtu.edu.cn

Jiale Yong

Dr Jiale Yong is currently a PhD candidate in Prof. Feng Chen's research group at Xi'an Jiaotong University. He received his BS degree from Xi'an Jiaotong University in 2011. His research interests include femtosecond laser microfabrication, controlling the wettability of solid surfaces, and bioinspired design of superhydrophobic and superoleophobic interfaces.

Feng Chen

Prof. Feng Chen is a full professor of Electronic Engineering at Xi'an Jiaotong University, where he directs the Femtosecond Laser Laboratory. He received a BS degree in physics from Sichuan University, China, in 1991, and then began to work for the Chinese Academy of Science (1991 to 2002), where he was promoted to a full professor in 1999. He received a PhD in Optics from the Chinese Academy of Science in 1997. In 2002, he joined Xi'an Jiaotong University, where he became a group leader. His current research interests are femtosecond laser microfabrication and bionic microfabrication.

Open Access Article. Published on 22 September 2015. Downloaded on 2/12/2026 6:34:48 AM.
This article is licensed under a Creative Commons Attribution 3.0 Unported Licence.

forms of anisotropic wettability. In addition, some intelligent surfaces show "smart wettability"; that is, the wettability of these surfaces can be reversibly switched through responding to external stimuli, such as light,[32,33] pH,[34,35] temperature,[36,37] electricity,[38,39] force,[40,41] *etc.* Smart wettability has been artificially achieved but is not observed in nature.[14] Up to now, many techniques have been developed to obtain the above-mentioned wettabilities, such as template imprinting,[42,43] self-assembly methods,[44,45] chemical etching,[46,47] photolithography,[48,49] plasma etching,[50,51] and electrospinning.[52,53]

In the past decade, femtosecond laser microfabrication has been applied in interface science to control the wettability of solid surfaces.[54–63] This technology can directly create micro/nanoscale hierarchical structures on a wide variety of materials by a simple one-step scanning method.[54,57,58,61,64] By combining a femtosecond laser system with a computer controlled three-dimensional translation stage, the laser processing position, scanning speed and scanning track can be precisely controlled by computer programs. Various pre-designed patterns have been prepared by this technology without the need for a harsh machining environment and expensive masks (Fig. 1). Since the wettability is governed by not only the chemical composition but also the surface topography, these pattern structures usually exhibit various special wetting properties.[65–68]

This paper provides an introduction to employing a femtosecond laser to realize special wettabilities. According to the characteristics of different wettabilities, we divide this article into four parts, which respectively focus on superhydrophobicity, underwater superoleophobicity, anisotropic wettability, and smart wettability. The formation mechanism of these properties is from simple to complex, while the function of these surfaces develops from single to multiple. With the price of femtosecond laser systems decreasing year by year, more and more laboratories have their own femtosecond laser equipment. This article should provide a useful guide for the integrated field of femtosecond laser microfabrication and wettability, and should attract more researchers to work on this interesting research area.

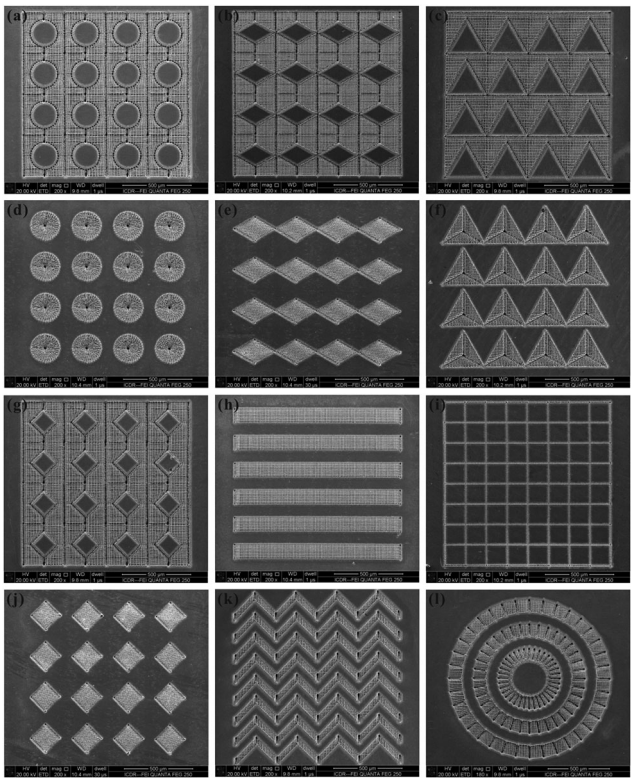

Fig. 1 Various patterns prepared through femtosecond laser microfabrication on a Ti sheet. (reproduced from ref. 58 with the permission of RSC)

2. Controlling wettability by a femtosecond laser

2.1 Superhydrophobicity

The most famous superhydrophobic surface is a lotus leaf whose surface is covered with micro/nanoscale hierarchical papillas and a hydrophobic wax crystal layer.[29,69] The combination of rough microstructures and hydrophobic chemistry endows the lotus leaf with water repellent ability because the

Qing Yang

Prof. Qing Yang received her BS degree in Photoelectron Science and Technology in 1992 from Sichuan University. In 2009, she received her PhD from Xi'an Institute of Optics and Fine Mechanics, Chinese Academy of Science. She is currently an associate professor at Xi'an Jiaotong University. Her current research interests are femtosecond laser fine process, microfluidic biochips, and micro-photonics.

Xun Hou

Prof. Xun Hou received his BS degree in Physics from Northwest University, China, in 1959. From Oct. 1979 to Nov. 1981, he worked at Imperial College in England as a visiting scholar. He was elected as an academician of the Chinese Academy of Sciences in 1991. He presently is a professor of Xi'an Jiaotong University, and he is also the director of the Shaanxi Key Laboratory of Photonics Technology for Information. His research interests mainly focus on photoelectronic materials and devices.

This journal is © The Royal Society of Chemistry 2015

Open Access Article. Published on 22 September 2015. Downloaded on 2/12/2026 6:34:48 AM.
This article is licensed under a Creative Commons Attribution 3.0 Unported Licence.

real contact area between a water droplet and the lotus leaf is greatly reduced. Inspired by nature, there are mainly two routes to design artificial superhydrophobic surfaces: modifying the rough surface using materials with a low surface energy and constructing rough microstructures on a hydrophobic substrate.[65–68]

Mazur *et al.* and Stratakis *et al.*, respectively, prepared superhydrophobic Si surfaces by femtosecond laser irradiation under reactive SF_6 gas.[70,71] The laser induced structure is composed of microscale conical spikes, arranging as a spike forest, as shown in Fig. 2a and b. The average size of the spikes is 10 μm and the aspect ratio is about 4. There are abundant nanoprotrusions with the size of a few hundred nanometers covering every spike. After fluoroalkylsilane modification, the two length-scale rough surface shows a WCA of $154^\circ \pm 1^\circ$ and a very small SA of $5^\circ \pm 2^\circ$. Both the artificial microstructure and the water-repellent characteristics are very similar to a natural lotus leaf.[71] However, SF_6 gas results in complex experimental equipment and a complicated fabrication process. It is of great significance to develop a simple way to prepare superhydrophobic surfaces in an ambient environment using a femtosecond laser.

We recently reported a self-organized rough micro-mountain array structure which was fabricated using a femtosecond laser on Si surface in an atmospheric environment, as shown in Fig. 2c–f.[72,73] The diameter and height of the rough micro-mountains are 6 μm and 2.9 μm, respectively. The micro-mountains arrange neatly and form a square array with a period of 10 μm. The surface roughness is about 2.46 μm. The inset in Fig. 2d shows the image of a 9 μL water droplet lying on the fluoroalkylsilane modified rough surface, with a WCA of $158^\circ \pm 1^\circ$. The water droplet on the surface can roll off easily as soon as the sample is tilted 4°. The surface shows superhydrophobicity and ultralow water adhesion, agreeing well with the Cassie contact state.[74,75] The water droplet only contacts the peak of the rough microstructures. An air cushion is trapped between the droplet and the rough surface. This air cushion endows the femtosecond laser induced surface with excellent water-repellent properties.

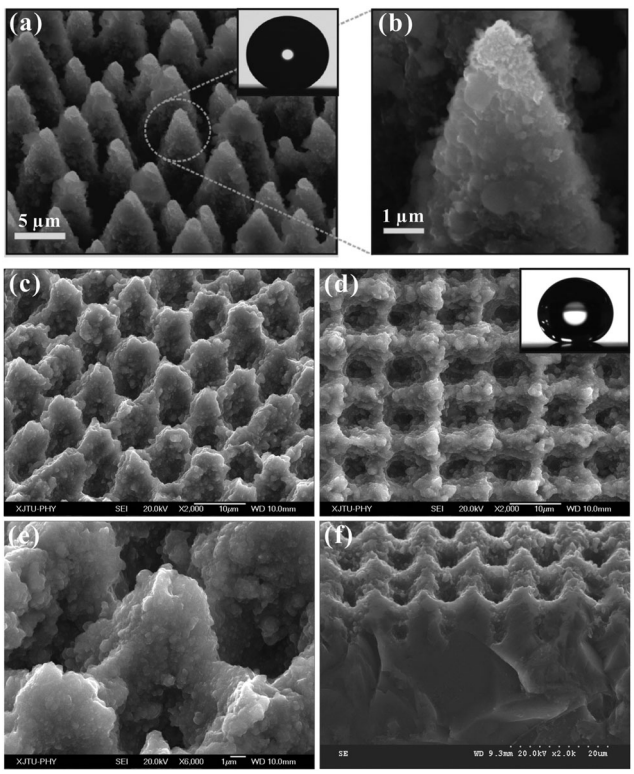

Fig. 2 Typical SEM images of the Si surfaces irradiated by a femtosecond laser under SF_6 gas (a and b) and in an air environment (c–f), respectively. The insets show a water droplet on the corresponding surfaces. (Reproduced from ref. 71 and 72 with the permission of Wiley and Springer.)

The as-prepared superhydrophobic surfaces possess excellent self-cleaning ability.[72] If the surfaces are polluted by calcium carbonate powder and slightly tilted, the water droplet located on the surface will roll off easily and take away the pollutants, leaving a clean path behind. Interestingly, the as-prepared surfaces still have superhydrophobicity for strong acid and alkaline solutions. This feature endows the surfaces with a self-cleaning function even in acid or alkaline rain. In addition, this pH stability makes the superhydrophobic surfaces promising for application in biological and chemical fields.

Superhydrophobicity can be directly achieved on hydrophobic materials without low surface energy modification compared with intrinsic hydrophilic substrates.[62] Fig. 3a shows the SEM image of the femtosecond laser irradiated polydimethylsiloxane (PDMS) surface. There are many flower-like particles with a size of several micrometers covering the surface. The particles are decorated with abundant nanoscale protrusions. The water droplet on the surface shows a static WCA of $162^\circ \pm 1^\circ$, and can roll off with the sample being tilted 1°. The superhydrophobicity with ultralow adhesion indicates that the droplet on the sample is in the Cassie state.[74,75]

We further weaved patterned PDMS surfaces consisting of a periodic square array based on selective femtosecond laser irradiation technology (Fig. 3b).[62] The femtosecond laser scanned domain is a micro/nanoscale hierarchical rough structure and shows ultralow adhesive superhydrophobicity. The rest of the non-irradiated flat PDMS surface exhibits intrinsic hydrophobicity (WCA = 110°). Fig. 3c shows the variation of WCA/SA with the length (L) of the side of the unstructured square when the period (T) of the square array is set at 200 μm. For a 7 μL water droplet, superhydrophobicity is obtained with $L \leq 180$ μm. For the patterned surface with a greater L, there is not enough laser irradiated rough area to realize superhydrophobicity; that is, the average roughness of the overall pattern surface is too low. The dynamic properties of a water droplet on the structured surface were also investigated *via* its sliding behavior. The water droplet moves easily on the surface with $L \leq 140$ μm as soon as the surface is only slightly tilted or shaken (Fig. 3d). As the L increases from 140 μm to 180 μm, the SA increases from $10^\circ \pm 1.5^\circ$ to $54^\circ \pm 3^\circ$ and then to 90° (Fig. 3e–g). SA = 90° means that the water droplet firmly pins on the sample even though the substrate is erected or turned upside down. The SA results reveal that the water adhesion of the superhydrophobic surfaces can be tuned from ultralow to ultrahigh. This adhesion controllability is realized by adjusting the area proportion of laser structured and non-structured regions, which show ultralow adhesion and

Open Access Article. Published on 22 September 2015. Downloaded on 2/12/2026 6:34:48 AM.
This article is licensed under a Creative Commons Attribution 3.0 Unported Licence.

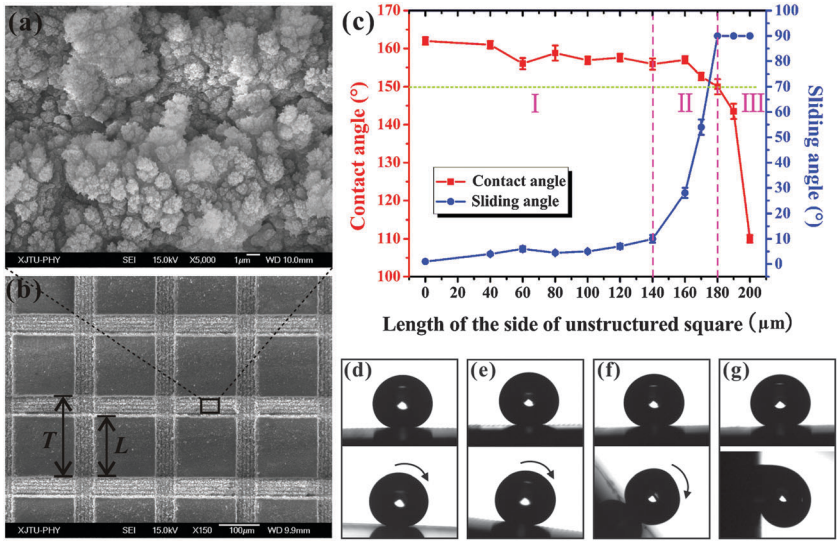

Fig. 3 (a) SEM image of the PDMS microstructure ablated by a femtosecond laser. (b) SEM image of the structured square array pattern. (c) WCA and SA values as a function of the L. (d–g) The shape and movement of a droplet on the square array surfaces: (d) L = 0 μm, (e) L = 140 μm, (f) L = 170 μm, and (g) L = 180 μm. (Reproduced from ref. 62 with the permission of ACS.)

ultrahigh adhesion, respectively. A water droplet on the heterogeneous patterned surfaces contacts both the flat and laser-induced rough domains. These two contact states are in Young and Cassie wetting models, respectively.[62] As the L increases, the area fraction of the laser structured domain (Cassie contact) will decrease. The decrease of the average surface roughness causes a decrease of the WCA. Whereas, the area fraction of the flat domain (Young contact) will increase, resulting in the increase of the water adhesion or SA value. Using these as-prepared surfaces, droplet rapid stop, small water droplet transfer, and controllable droplet bounce are achieved.[62] In addition, many other microstructures and patterns are also prepared and showed controllable adhesive superhydrophobicity.[61,63,76]

2.2 Underwater superoleophobicity

Fish can swim freely in oil-spill water and avoid being polluted by oil because of the underwater superoleophobicity of their skin.[77] The unique ability is found from the synergy between the hierarchical rough microstructures and the hydrophilic chemistry of fish scales. The characteristic of fish scales suggests that surfaces that are superhydrophilic in air are generally superoleophobic in water.

Femtosecond laser ablated micro-mountain array structures on an Si surface (without fluoroalkylsilane modification) can also be used to obtain underwater superoleophobicity.[56] A flat Si surface shows weak hydrophilicity in air with a WCA of 60° (Fig. 4a). If the flat sample is immersed in water, more than half of an oil droplet (1,2-dichloroethane) on the surface will retain a nearly spherical shape (Fig. 4c). The OCA is 124.6° ± 1°, showing ordinary oleophobicity in water. After femtosecond laser ablation, the wettability of the sample is enhanced by the hierarchical rough microstructures. The water droplet can spread out quickly on the laser ablated surface, exhibiting superhydrophilicity with a WCA of 4° in air (Fig. 4b). Interestingly, the laser induced

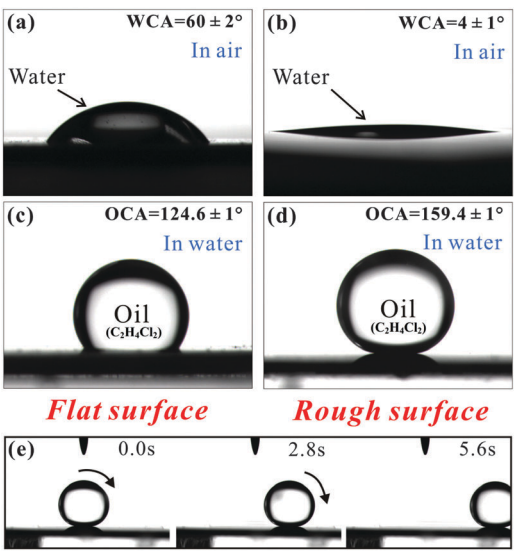

Fig. 4 (a–d) Water wettability in air and underwater oil wettability of a flat Si surface and a laser induced rough Si surface, respectively. (e) Underwater oil droplet rolling on a laser ablated sample tilted 0.5°. (Reproduced from ref. 56 with the permission of RSC.)

surface shows superoleophobicity in water. The oil droplet can retain a spherical shape on the sample surface in water medium (Fig. 4d). The OCA reaches up to 159.4° ± 1°. The surface also achieves ultralow oil adhesion in water since the oil droplet can roll easily on a 0.5° tilted structured surface (Fig. 4e). According to the underwater version of the Cassie model, the rough microstructure is fully wetted by water.[56,77] The underwater oil droplet is supported by the micro-mountains and only touches the tip of the rough microstructures. A water cushion is trapped below the oil droplet. The trapped water endows the surface with underwater superoleophobicity because water naturally repels oil.

 This journal is © The Royal Society of Chemistry 2015

Open Access Article. Published on 22 September 2015. Downloaded on 2/12/2026 6:34:48 AM.
This article is licensed under a Creative Commons Attribution 3.0 Unported Licence.

Ultralow oil adhesion is a result of a small contact area between the underwater oil droplet and the rough substrate. Hydrophilic silicon in air becomes oleophobic in water, while the oleophobicity is greatly amplified into underwater superoleophobicity by femtosecond laser induced rough microstructures.

Transparent underwater superoleophobicity was also realized on a silica glass surface.[57] Achieving underwater superoleophobicity and light transmission are inspired by fish scales and *Diphylleia grayi*, respectively. The petals of *Diphylleia grayi* are white in air, but upon contact with water (such as in the rain) they become transparent, as shown in Fig. 5a and b.[57] Because of the loose cell structure, water can enter the intercellular space of *Diphylleia grayi* petals on rainy days. A water–water interface displaces the initial water–air interface (in air), increasing light transmission so the petals turn transparent. Fig. 5c shows the microstructure of the femtosecond laser ablated silica glass surface. Abundant irregular nano-particles disorderly distribute on the surface. When the laser ablated silica glass is immersed in water, the oil droplet on it retains a spherical shape (Fig. 5d). The OCA reaches up to 160.2° ± 1°, while the SA is only 1°, revealing an underwater superoleophobicity with ultralow oil-adhesion.

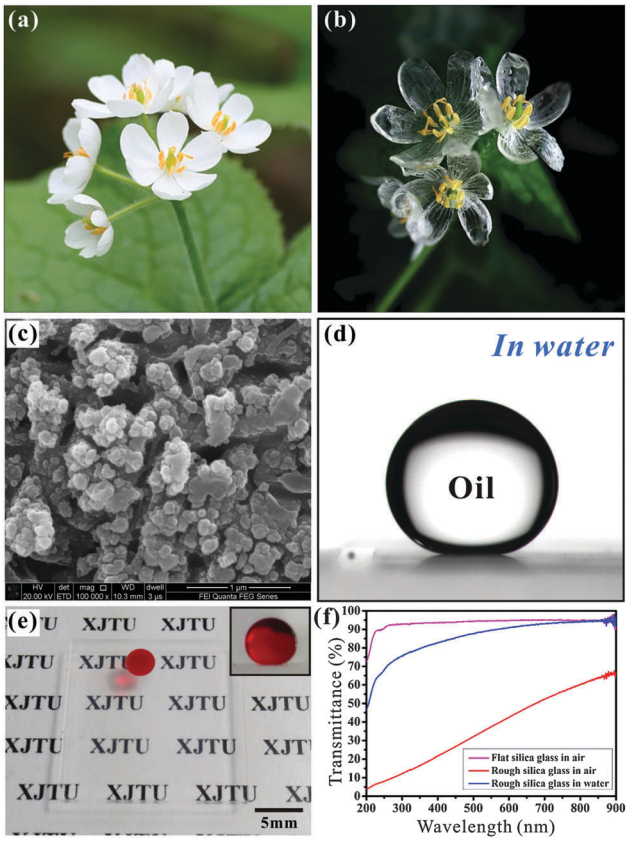

Fig. 5 (a and b) Petals of *Diphylleia grayi*: (a) on a sunny day; (b) in the rain. (c) SEM image of the femtosecond laser irradiated silica glass surface. (d) An underwater oil droplet on femtosecond laser irradiated silica glass. (e) High transparency of the laser induced surface in water medium. (f) UV-vis spectra of various silica glasses. (Reproduced from ref. 57 with the permission of RSC.)

The transmittance of rough silica glass is improved by shifting from the atmosphere to water medium. When we put paper with black letters behind the laser induced glass, the letters look obscure in air. After putting the sample in water, the letters "XJTU" become very clear (Fig. 5e). The underwater oil droplet on the sample remains a small sphere (inset of Fig. 5e). The remarkable transparency is confirmed by UV-vis spectra (Fig. 5f). The underwater structured surface has a similar transmittance to bare flat silica glass in the visible region. The water environment plays an important role in obtaining this good transparency. Similar to the *Diphylleia grayi* petals becoming transparent in the rain, the rough nanoscale structure of silica glass is wetted by water by immersing in water, forming a glass–water interface instead of a glass–air interface. Since the refractive index of water is closer to that of silica glass than to that of air, the degree of Mie scattering is effectively weakened, resulting in excellent transparency.[78,79]

Controllable underwater oil-adhesion was realized on femtosecond laser ablated ordinary glass surfaces.[80] The resultant surfaces show a micro/nanoscale binary rough topography and underwater superoleophobicity. By increasing the average distance of the laser pulse focus, the underwater oil-adhesion increases from ultralow to ultrahigh because the oil droplet on the structured surfaces changes from the underwater Cassie state to the metastable state, and then to the underwater Wenzel state. The superoleophobic surface with low oil-adhesion is an ideal anti-oil-contamination layer in water. The superoleophobic surface with ultrahigh oil-adhesion can be applied in oil droplet transfer and even in the fusion of oil/organic microdroplets.

2.3 Anisotropic wettability

A slow femtosecond laser scan leaves a microgroove on a substrate surface. Using the line-by-line scanning mode, we obtained a periodic microgroove array on a PDMS substrate, as shown in Fig. 6a.[55] Every microgroove has a width of 12.17 μm and a depth of 8.57 μm. In addition, many irregular nanoscale particles randomly decorate on the inner wall and outer rim of the microgrooves.

A water droplet on the microgroove array structure is stretched along the microgrooves (Fig. 6b). The anisotropic wettability of the groove-like microstructure is usually studied by measuring the perpendicular and parallel WCA/SA values.[30,73,81–83] The WCAs (SAs) perpendicular to and parallel to the microgrooves, respectively, are defined as $WCA_{\perp}$ and $WCA_{\parallel}$ ($SA_{\perp}$ and $SA_{\parallel}$). Fig. 6c shows the parallel view of a water droplet on the microgroove array surface with a period (D) of 150 μm. The $WCA_{\parallel}$ is 116.5° ± 2.5°, whereas the droplet along the perpendicular direction has a higher contact angle and the $WCA_{\perp}$ is 134.8° ± 2.5° (Fig. 6d). The degree of wetting anisotropy, $WCA_{\perp} - WCA_{\parallel}$, is about 18.3°. Three main factors cause this anisotropic wetting phenomenon. Firstly, an energy barrier usually forms at the boundary between the laser-induced microgroove and the non-irradiated flat PDMS domain.[73,83,84] This energy barrier can prevent the water droplet from spreading along the perpendicular direction, while there is no energy barrier along the parallel direction. Secondly, the water droplet

Open Access Article. Published on 22 September 2015. Downloaded on 2/12/2026 6:34:48 AM.
This article is licensed under a Creative Commons Attribution 3.0 Unported Licence.

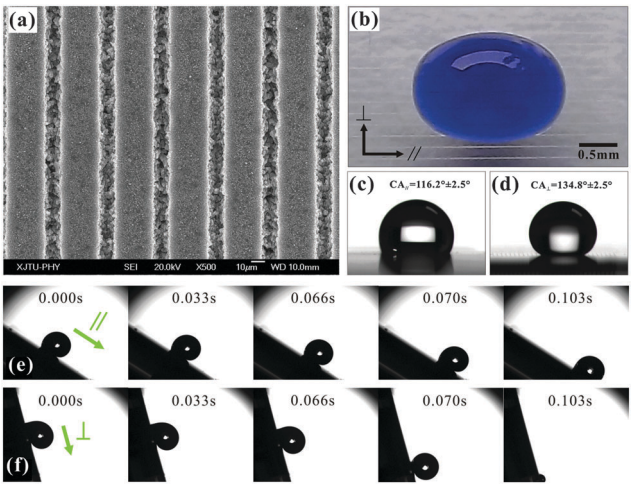

Fig. 6 (a) SEM image of a femtosecond laser induced microgroove array with D = 40 μm. (b) A blue-dyed water droplet on a microgroove array surface. (c and d) A water droplet on a microgroove patterned surface (D = 150 μm) viewed from the parallel (c) and perpendicular (d) directions. (e and f) Droplet rolling on the microgroove array (D = 25 μm) along the parallel and perpendicular directions. The sample is titled 31° (e) and 76° (f), respectively. (Reproduced from ref. 55 with the permission of RSC.)

can partly dive into the rough microgrooves and is further driven to flow along the microgrooves by capillary action.[85–90] Finally, the three-phase contact line (TCL) is continuous along the microgrooves.[91] It is better for the droplet spreading and moving forward.

Fig. 6e and f describe the rolling process of a water droplet on the microgroove array surface (D = 25 μm) along the parallel and perpendicular directions, respectively. The $SA_{\parallel}$ is 31° ± 3°, while the $SA_{\perp}$ is about 76° ± 5°. The results show that the droplet prefers to move along the groove direction. The SA difference reaches up to 45°, but the value of a rice leaf is only 6°. A continuous short TCL always endows the surfaces with excellent water-shedding properties.[91] The water droplet on the microgroove structure has a continuous TCL along the parallel direction. However, the TCL along the perpendicular direction is very discontinuous and looks longer. A stronger hysteresis effect forms in the perpendicular direction, resulting in the water droplet rolling along this direction being more difficult than along the parallel direction.

A femtosecond laser induced microgroove array structure can also be immersed in water to control oil wettability.[92] We fabricated a similar microgroove array on a Si substrate and realized underwater anisotropic oil-wetting. For the sample with D = 450 μm, the OCAs parallel to and perpendicular to the grooves are 135.7° ± 1.5° and 155.5° ± 1.6°, respectively. The contact angle along the parallel direction is significantly smaller than that along the perpendicular direction, revealing that the oil droplet tends to spread along the microgrooves. The degree of wetting anisotropy can be controlled from 0° to 19.8° by the period of the microgroove arrays.

A butterfly avoids being "shot down" by raindrops due to the directional adhesion of its wings.[93] Inspired by butterfly wings, a kind of triangle array pattern was constructed on PDMS material based on selective femtosecond laser irradiation.[94] The untreated triangle array is flat hydrophobic PDMS, while the surrounding domain is induced by a femtosecond laser and shows superhydrophobicity. The droplet on the sample rolls along one direction distinctly easier than its opposite direction when the droplet and a single hydrophobic triangle have a comparable size. This special anisotropic wettable phenomenon is usually called "directional adhesion".[93] The obtained sliding anisotropy can even reach up to 21°. The directional adhesion results from the direction-dependent arrangement of hydrophobic triangles because the water droplets rolling along those two opposite directions have different TCL situations.

2.4 Smart wettability

Switchable wettability has been realized on femtosecond laser ablated Ti surfaces.[58] As shown in Fig. 7a and b, the laser induced morphology is typical rough micro-mountain arrays. The laser ablated sample consists of both Ti and a new element O instead of pure Ti. Their atomic proportions are 51.81% and 48.19%, respectively. Oxidation and hierarchical rough microstructure formation synchronously happen during the femtosecond laser ablation, constructing a rough TiO_2 layer covering on the original substrate.

The laser-induced surface initially shows superhydrophobicity with a WCA of 154.5° ± 2.5° (Fig. 7c). A mirror-like interface can be seen by immersing the sample in water, revealing that the laser-irradiated Ti is a Cassie surface.[95] After UV irradiation for 40 min, the WCA decreases to 2.5° (Fig. 7d). At present, the sample submerged in water does not show a silver mirror. The wettability is switched from superhydrophobicity to superhydrophilicity in air. Furthermore, the sample can re-obtain superhydrophobicity through dark storage for 2 days.

The switching trend of oil wettability in water is opposite to that of water wettability in air. The laser-induced sample incipiently presents underwater superoleophilicity (Fig. 7e). The underwater oil droplet will spread out quickly with an OCA of nearly 4° once it contacts the submerged rough TiO_2 surface. After UV light irradiation, the wettability of the sample switches to underwater superoleophobicity (Fig. 7f). The underwater oil droplet on the sample has an OCA of 160.5° ± 2° and can easily roll away if the sample is titled 1°. The underwater superoleophilicity can also be recovered by keeping the sample in the dark for 2 days. Both the water wettability and the underwater oil wettability can be cycled many times. A similar property is also seen on the femtosecond laser treated Zn surface.[59]

As shown in Fig. 7g, femtosecond laser irradiation not only generates hierarchical rough microstructures but also oxidizes the Ti material. The laser induced rough TiO_2 layer shows ultralow water adhesive superhydrophobicity. According to the Cassie model, the water droplet only contacts the peak of the rough microstructures (Fig. 7i).[74–76] An air cushion forms between the water droplet and the rough sample surface by submerging the as-prepared sample in water. When an underwater oil droplet contacts the surface, the oil will spread along and displace the trapped air due to the pressure and capillary action, resulting in underwater superoleophilicity (Fig. 7k). During UV light irradiation, lattice oxygen combines with photogenerated

 This journal is © The Royal Society of Chemistry 2015

Open Access Article. Published on 22 September 2015. Downloaded on 2/12/2026 6:34:48 AM.
This article is licensed under a Creative Commons Attribution 3.0 Unported Licence.

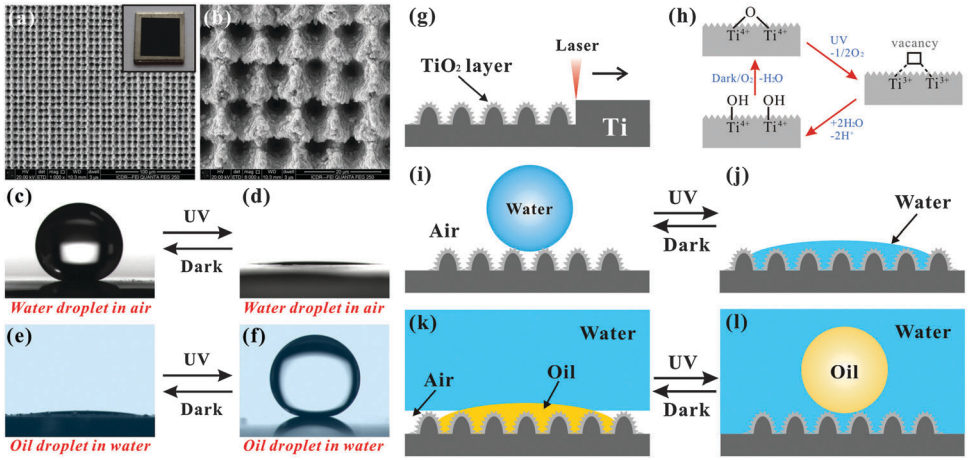

Fig. 7 (a and b) SEM images of the Ti surface irradiated by a femtosecond laser. (c–f) Reversible switching superhydrophobicity–superhydrophilicity and underwater superoleophilicity–superoleophobicity through alternate UV irradiation and dark storage. (g–l) A schematic illustration of the switchable wettability. (Reproduced from ref. 58 with the permission of RSC.)

holes to form oxygen vacancies on a TiO_2 surface.[96–101] The oxygen vacancies further turn into hydroxyl groups by dissociative adsorption of atmospheric water (Fig. 7h). The hydroxyl groups make the rough TiO_2 surface exhibit superhydrophilicity (Fig. 7j). Upon immersing the sample in water, the microstructures are completely wetted and occupied by water. If an oil droplet is placed on the sample surface, a water cushion will be trapped between the oil droplet and the substrate (Fig. 7l). The water cushion endows the sample with underwater superoleophobicity based on the underwater version of the Cassie contact model.[56,77] For the dark storage process, the implanted hydroxyl moieties tend to be replaced by ambient oxygen.[96,97] As the hydrophobicity grows stronger, the sample recovers its original superhydrophobic and underwater superoleophilic state (Fig. 7i and k).

With the aid of underwater superoleophobicity and ultralow oil-adhesion of femtosecond laser induced rough Si surfaces, an *in situ* "mechanical hand" for oil droplet transportation was realized in water through switching the density (ρ) of the water solution.[60] As shown in Fig. 8a, the setup mainly consists of one water container and two underwater superoleophobic samples (femtosecond laser irradiated Si surfaces). The whole transportation process (Fig. 8b) was performed in a water environment. A 15 μL oil droplet (ρ = 1.26 g cm^{-3}) was firstly located on the below sample (Step 1). The above sample was lowered down until it just touched the oil droplet (Step 2). Next, sugar water (ρ = 1.52 g cm^{-3}) was slowly poured into the glass container to increase the ρ of the water solution, switching the oil droplet from heavier to lighter than the surrounding water solution (Step 3). The oil droplet became brighter because sugar water has a refractive index closer to the oil droplet than deionized water. If we lifted the above sample up, the oil droplet would be picked up since the gravity was less than the buoyancy acting on the oil droplet (Step 4). Interestingly, we can also put the oil droplet back onto the below sample by taking an opposite approach. Firstly, the above sample was lowered down so that the hanging oil droplet touched the below sample again (Step 5). Then, the water solution in the container was diluted

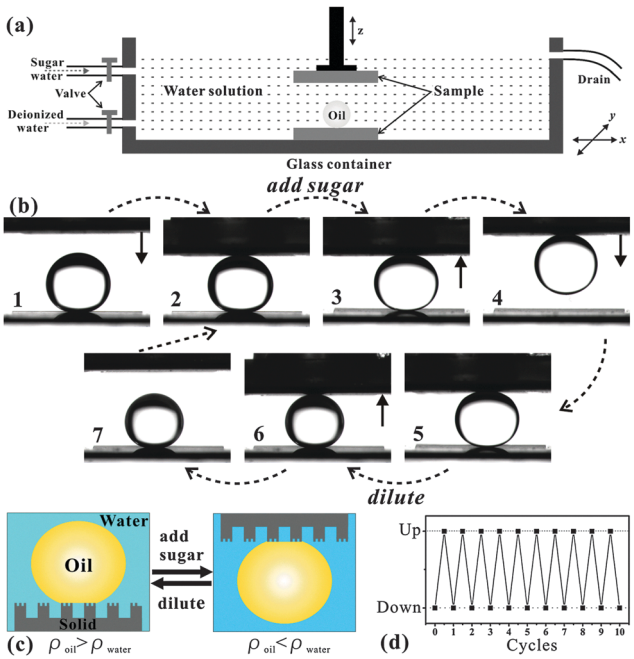

Fig. 8 Underwater oil droplet transportation by underwater superoleophobic surfaces. (a) A schematic of the setup. (b) The operational process of "picking up" and "putting down" an oil droplet in water medium. (c and d) Reversibility and repeatability of the no-loss oil droplet transportation. (Reproduced from ref. 60 with the permission of Wiley.)

by deionized water to become much lighter than the oil droplet until it again turned very transparent (Step 6). The underwater oil droplet also recovered its original brightness. Finally, by lifting the above sample up, the oil droplet detached from the above sample and stayed on the surface below (Step 7). The oil droplet can be picked up when the oil is lighter than the water environment, while it can be put down when the oil is heavier than the water environment (Fig. 8c). This reversible transportation can be repeated over many cycles and has almost no oil loss (Fig. 8d).

Open Access Article. Published on 22 September 2015. Downloaded on 2/12/2026 6:34:48 AM. This article is licensed under a Creative Commons Attribution 3.0 Unported Licence.

3. Conclusions

This paper introduces some recent developments in achieving special wettability through femtosecond laser microfabrication. Using different materials and machining methods, we can design the rough microstructure, pattern, and even chemistry on solid substrates. Superhydrophobicity, underwater superoleophobicity, anisotropic wettability, and smart wettability have been obtained. A micro-mountain array structure is built on a Si surface by femtosecond laser irradiation. After fluoroalkylsilane modification, the sample shows superhydrophobicity and ultralow water adhesion. Superhydrophobicity can also be directly obtained on hydrophobic materials, such as PDMS, without modification by a low surface energy. In addition to superhydrophobicity, the femtosecond laser induced rough Si surface also exhibits superoleophobicity when the sample is immersed in water. A microgroove array structure is prepared by a line-by-line scanning process, and the resultant surface achieves anisotropic wetting and anisotropic sliding, being similar to the natural rice leaf. For some materials like Ti, an oxidation process also happens with rough microstructure formation during femtosecond laser ablation. The generated rough TiO_2 layer exhibits smart wettability; that is, superhydrophobicity–superhydrophilicity, as well as underwater superoleophilicity–superoleophobicity, can be reversibly switched by alternate UV irradiation and dark storage. We believe that the combination of wettability and a femtosecond laser will have important potential applications in droplet/fluid manipulation, microfluidics, biomedicine, chemical and biological sensing, *etc.*

Acknowledgements

This work was supported by the National Science Foundation of China under Grant No. 61275008, 51335008 and 61435005, and the special-funded programme of National Key Scientific Instruments and Equipment Development of China under Grant No. 2012YQ12004706.

References

1 K. Liu, X. Yao and L. Jiang, *Chem. Soc. Rev.*, 2010, **39**, 3240–3255.
2 F. Xia and L. Jiang, *Adv. Mater.*, 2008, **20**, 2842–2858.
3 T. Darmanin and F. Guittard, *J. Mater. Chem. A*, 2014, **2**, 16319–16359.
4 X. Yao, Y. Song and L. Jiang, *Adv. Mater.*, 2011, **23**, 719–734.
5 Z. Xue, Y. Cao, N. Liu, L. Feng and L. Jiang, *J. Mater. Chem. A*, 2014, **2**, 2445–2460.
6 B. Bhushan, *Philos. Trans. R. Soc., A*, 2009, **367**, 1445–1486.
7 N. J. Shirtcliffe, G. McHale and M. I. Newton, *J. Polym. Sci., Part B: Polym. Phys.*, 2011, **49**, 1203–1217.
8 Y. Zhang, Y. Chen, L. Shi, J. Li and Z. Guo, *J. Mater. Chem.*, 2012, **22**, 799–815.
9 P. Ragesh, V. A. Ganesh, S. V. Nair and A. S. Nair, *J. Mater. Chem. A*, 2014, **2**, 14773–14797.
10 Y. L. Zhang, Q. D. Chen, Z. Jin, E. Kim and H. B. Sun, *Nanoscale*, 2012, **4**, 4858–4869.
11 Y. Tian, B. Su and L. Jiang, *Adv. Mater.*, 2014, **26**, 6872–6897.
12 B. Chang, M. Zhang, G. Qing and T. Sun, *Small*, 2015, **11**, 1097–1112.
13 M. Liu and L. Jiang, *Adv. Funct. Mater.*, 2010, **20**, 3753–3764.
14 X. Liu, Y. Liang, F. Zhou and W. Liu, *Soft Matter*, 2012, **8**, 2070–2086.
15 Y. Wu, Q. Wei, M. Cai and F. Zhou, *Adv. Mater. Interf.*, 2015, **2**, 1400392.
16 T. Sun and G. Qing, *Adv. Mater.*, 2011, **23**, H57–H77.
17 Y. L. Zhang, H. Xia, E. Kim and H. B. Sun, *Soft Matter*, 2012, **8**, 11217–11231.
18 S. Nishimoto and B. Bhushan, *RSC Adv.*, 2013, **3**, 671–690.
19 X. Zhang, L. Wang and E. Levänen, *RSC Adv.*, 2013, **3**, 12003–12020.
20 E. Stratakis, A. Rannella and C. Fotakis, *Biomicrofluidics*, 2011, **5**, 013411.
21 Z. Chu and S. Seeger, *Chem. Soc. Rev.*, 2014, **43**, 2784–2798.
22 L. Wen, Y. Tian and L. Jiang, *Angew. Chem., Int. Ed.*, 2015, **54**, 3387–3399.
23 H. Teisala, M. Tuominen and J. Kuusipalo, *Adv. Mater. Interfaces*, 2014, **1**, 1300026.
24 X. M. Li, D. Reinhoudt and M. Crego-Calama, *Chem. Soc. Rev.*, 2007, **36**, 1350–1368.
25 T. Jiang, Z. Guo and W. Liu, *J. Mater. Chem. A*, 2015, **3**, 1811–1827.
26 A. K. Kota, J. M. Mabry and A. Tuteja, *Surf. Innovations*, 2013, **1**, 71–83.
27 Z. Xue, M. Liu and L. Jiang, *J. Polym. Sci., Part B: Polym. Phys.*, 2012, **50**, 1209–1224.
28 X. Liu, J. Zhou, Z. Xue, J. Gao, J. Meng, S. Wang and L. Jiang, *Adv. Mater.*, 2012, **24**, 3401–3405.
29 L. Feng, S. Li, Y. Li, H. Li, L. Zhang, J. Zhai, Y. Song, B. Liu, L. Jiang and D. Zhu, *Adv. Mater.*, 2002, **14**, 1857–1860.
30 S. Z. Wu, D. Wu, J. Yao, Q. D. Chen, J. N. Wang, L. G. Niu, H. H. Fang and H. B. Sun, *Langmuir*, 2010, **26**, 12012–12016.
31 D. Wu, J. N. Wang, S. Z. Wu, Q. D. Chen, S. Zhao, H. Zhang, H. B. Sun and L. Jiang, *Adv. Funct. Mater.*, 2011, **21**, 2927–2932.
32 D. Wang, Y. Liu, X. Liu, F. Zhou, W. Liu and Q. Xue, *Chem. Commun.*, 2009, 7018–7020.
33 D. Wang, X. Wang, X. Liu and F. Zhou, *J. Phys. Chem. C*, 2010, **114**, 9938–9944.
34 L. Zhang, Z. Zhang and P. Wang, *NPG Asia Mater.*, 2012, **4**, e8.
35 Z. Cheng, H. Lai, Y. Du, K. Fu, R. Hou, C. Li, N. Zhang and K. Sun, *ACS Appl. Mater. Interfaces*, 2014, **6**, 636–641.
36 T. Sun, G. Wang, L. Feng, B. Liu, Y. Ma, L. Jiang and D. Zhu, *Angew. Chem., Int. Ed.*, 2004, **43**, 357–360.
37 F. Xia, L. Feng, S. Wang, T. Sun, W. Song, W. Jiang and L. Jiang, *Adv. Mater.*, 2006, **18**, 432–436.
38 S. Lee, W. Kim and K. Yong, *Adv. Mater.*, 2011, **23**, 4398–4402.

 This journal is © The Royal Society of Chemistry 2015

Open Access Article. Published on 22 September 2015. Downloaded on 2/12/2026 6:34:48 AM. This article is licensed under a Creative Commons Attribution 3.0 Unported Licence.

39 X. Hong, X. Gao and L. Jiang, *J. Am. Chem. Soc.*, 2007, **129**, 1478–1479.
40 D. Wu, S. Z. Wu, Q. D. Chen, Y. L. Zhang, J. Yao, X. Yao, L. G. Niu, J. N. Wang, L. Jiang and H. B. Sun, *Adv. Mater.*, 2011, **23**, 545–549.
41 S. Zhao, H. Xia, D. Wu, C. Lv, Q. D. Chen, K. Ariga, L. Q. Liu and H. B. Sun, *Soft Matter*, 2013, **9**, 4236–4240.
42 P. Guo, Y. Zheng, C. Liu, J. Ju and L. Jiang, *Soft Matter*, 2012, **8**, 1770–1775.
43 Y. Cai, L. Lin, Z. Xue, M. Liu, S. Wang and L. Jiang, *Adv. Funct. Mater.*, 2014, **24**, 809–816.
44 Y. Li, E. J. Lee and S. O. Cho, *J. Phys. Chem. C*, 2007, **111**, 14813–14817.
45 Y. Li, X. J. Huang, S. H. Heo, C. C. Li, Y. K. Choi, W. P. Cai and S. O. Cho, *Langmuir*, 2007, **23**, 2169–2174.
46 J. Li, X. Liu, Y. Ye, H. Zhou and J. Chen, *J. Phys. Chem. C*, 2011, **115**, 4726–4729.
47 Z. Cheng, H. Lai, Y. Du, K. Fu, R. Hou, N. Zhang and K. Sun, *ACS Appl. Mater. Interfaces*, 2013, **5**, 11363–11370.
48 D. Wu, S. Z. Wu, Q. D. Chen, S. Zhao, H. Zhang, J. Jiao, J. A. Piersol, J. N. Wang, H. B. Sun and L. Jiang, *Lab Chip*, 2011, **11**, 3873–3879.
49 M. Im, H. Im, J. H. Lee, J. B. Yoon and Y. K. Choi, *Soft Matter*, 2010, **6**, 1401–1404.
50 E. Bormashenko, R. Grynyov, Y. Bormashenko and E. Drori, *Sci. Rep.*, 2012, **2**, 741.
51 J. Zhang and S. Seeger, *Angew. Chem., Int. Ed.*, 2011, **50**, 6652–6656.
52 M. Guo, B. Ding, X. Li, X. Wang, J. Yu and M. Wang, *J. Phys. Chem. C*, 2010, **114**, 916–921.
53 H. S. Lim, J. H. Baek, K. Park, H. S. Shin, J. Kim and J. H. Cho, *Adv. Mater.*, 2010, **22**, 2138–2141.
54 F. Chen, D. Zhang, Q. Yang, J. L. Yong, G. Du, J. Si, F. Yun and X. Hou, *ACS Appl. Mater. Interfaces*, 2013, **5**, 6777–6792.
55 J. L. Yong, Q. Yang, F. Chen, D. Zhang, U. Farooq, G. Du and X. Hou, *J. Mater. Chem. A*, 2014, **2**, 5499–5507.
56 J. L. Yong, F. Chen, Q. Yang, D. Zhang, U. Farooq, G. Du and X. Hou, *J. Mater. Chem. A*, 2014, **2**, 8790–8795.
57 J. L. Yong, F. Chen, Q. Yang, G. Du, C. Shan, H. Bian, U. Farooq and X. Hou, *J. Mater. Chem. A*, 2015, **3**, 9379–9384.
58 J. L. Yong, F. Chen, Q. Yang, U. Farooq and X. Hou, *J. Mater. Chem. A*, 2015, **3**, 10703–10709.
59 J. L. Yong, F. Chen, Q. Yang, Y. Fang, J. Huo and X. Hou, *Chem. Commun.*, 2015, **51**, 9813–9816.
60 J. L. Yong, Q. Yang, F. Chen, H. Bian, G. Du, U. Farooq and X. Hou, *Adv. Mater. Interfaces*, 2015, **2**, 1400388.
61 D. Zhang, F. Chen, Q. Yang, J. L. Yong, H. Bian, Y. Ou, J. Si, X. Meng and X. Hou, *ACS Appl. Mater. Interfaces*, 2012, **4**, 4905–4912.
62 J. L. Yong, F. Chen, Q. Yang, D. Zhang, G. Du, J. Si, F. Yun and X. Hou, *J. Phys. Chem. C*, 2013, **117**, 24907–24912.
63 J. L. Yong, F. Chen, Q. Yang, D. Zhang, H. Bian, G. Du, J. Si, X. Meng and X. Hou, *Langmuir*, 2013, **29**, 3274–3279.
64 J. L. Yong, F. Chen, Q. Yang, G. Du, H. Bian, D. Zhang, J. Si, F. Yun and X. Hou, *ACS Appl. Mater. Interfaces*, 2013, **5**, 9382–9385.
65 P. Roach, N. J. Shirtcliffe and M. I. Newton, *Soft Matter*, 2008, **4**, 224–240.
66 K. Liu and L. Jiang, *Nano Today*, 2011, **6**, 155–175.
67 C. H. Xue and J. Z. Ma, *J. Mater. Chem. A*, 2013, **1**, 4146–4161.
68 M. Nosonovsky and B. Bhushan, *J. Phys.: Condens. Matter*, 2008, **20**, 225009.
69 W. Barthlott and C. Neinhuis, *Planta*, 1997, **202**, 1–8.
70 T. Baldacchini, J. E. Carey, M. Zhou and E. Mazur, *Langmuir*, 2006, **22**, 4917–4919.
71 V. Zorba, E. Stratakis, M. Barberoglou, E. Spanakis, P. Tzanetakis, S. Anastasiadis and C. Fotakis, *Adv. Mater.*, 2008, **20**, 4049–4054.
72 J. L. Yong, Q. Yang, F. Chen, D. Zhang, H. Bian, Y. Ou, G. Du and X. Hou, *Appl. Phys. A: Mater. Sci. Process.*, 2013, **111**, 243–249.
73 F. Chen, D. Zhang, Q. Yang, X. Wang, B. Dai, X. Li, X. Hao, Y. Ding, J. Si and X. Hou, *Langmuir*, 2011, **27**, 359–365.
74 A. B. D. Cassie and S. Baxter, *Trans. Faraday Soc.*, 1944, **40**, 546–551.
75 S. Wang and L. Jiang, *Adv. Mater.*, 2007, **19**, 3423–3424.
76 J. L. Yong, Q. Yang, F. Chen, D. Zhang, G. Du, H. Bian, J. Si, F. Yun and X. Hou, *Appl. Surf. Sci.*, 2014, **288**, 579–583.
77 M. Liu, S. Wang, Z. Wei, Y. Song and L. Jiang, *Adv. Mater.*, 2009, **21**, 665–669.
78 X. Deng, L. Mammen, H. J. Butt and D. Vollmer, *Science*, 2012, **335**, 67–70.
79 P. A. Levkin, F. Svec and J. M. J. Fréchet, *Adv. Funct. Mater.*, 2009, **19**, 1993–1998.
80 J. L. Yong, F. Chen, Q. Yang, U. Farooq, H. Bian, G. Du and X. Hou, *Appl. Phys. A: Mater. Sci. Process.*, 2015, **119**, 837–844.
81 M. Gleiche, L. F. Chi and H. Fuchs, *Nature*, 2000, **403**, 173–175.
82 S. G. Park, J. H. Moon, H. C. Jeon and S. M. Yang, *Soft Matter*, 2012, **8**, 4567–4570.
83 E. Mele, S. Girardo and D. Pisignano, *Langmuir*, 2012, **28**, 5312–5317.
84 J. Y. Chung, J. P. Youngblood and C. M. Stafford, *Soft Matter*, 2007, **3**, 1163–1169.
85 A. Y. Vorobyev and C. L. Guo, *Appl. Phys. Lett.*, 2009, **94**, 224102.
86 Y. M. Zheng, H. Bai, Z. B. Huang, X. L. Tian, F. Q. Niu, Y. Zhao, J. Zhai and L. Jiang, *Nature*, 2010, **463**, 640–643.
87 J. C. Baret and M. M. J. Decré, *Langmuir*, 2007, **23**, 5200–5204.
88 J. Ju, H. Bai, Y. M. Zheng, T. Y. Zhao, R. C. Fang and L. Jiang, *Nat. Commun.*, 2012, **3**, 1247.
89 A. Y. Vorobyev and C. L. Guo, *J. Appl. Phys.*, 2010, **108**, 123512.
90 K. Khare, S. Herminghaus, J. C. Baret, B. M. Law, M. Brinkmann and R. Seemann, *Langmuir*, 2007, **23**, 12997–13006.
91 Z. Yoshimitsu, A. Nakajima, T. Watanabe and K. Hashimoto, *Langmuir*, 2002, **18**, 5818–5822.

Open Access Article. Published on 22 September 2015. Downloaded on 2/12/2026 6:34:48 AM.
This article is licensed under a Creative Commons Attribution 3.0 Unported Licence.

92 J. L. Yong, F. Chen, Q. Yang, U. Farooq, H. Bian, G. Du and X. Hou, *Appl. Phys. Lett.*, 2014, **105**, 071608.
93 Y. Zheng, X. Gao and L. Jiang, *Soft Matter*, 2007, **3**, 178–182.
94 J. L. Yong, Q. Yang, F. Chen, D. Zhang, G. Du, H. Bian, J. Si and X. Hou, *RSC Adv.*, 2014, **4**, 8138–8143.
95 I. A. Larmour, S. E. J. Bell and G. C. Saunders, *Angew. Chem.*, 2007, **119**, 1740–1742.
96 K. Liu, M. Cao, A. Fujishima and L. Jiang, *Chem. Rev.*, 2014, **114**, 1044–1094.
97 R. Wang, K. Hashimoto, A. Fujishima, M. Chikuni, E. Kojima, A. Kitamura, M. Shimohigoshi and T. Watanabe, *Nature*, 1997, **388**, 431–433.
98 Y. Li, G. Duan, G. Liu and W. Cai, *Chem. Soc. Rev.*, 2013, **42**, 3614–3627.
99 Y. Li, T. Sasaki, Y. Shimizu and N. Koshizaki, *J. Am. Chem. Soc.*, 2008, **130**, 14755–14762.
100 Y. Li, N. Koshizaki, H. Wang and Y. Shimizu, *ACS Nano*, 2011, **5**, 9403–9412.
101 Y. Li, T. Sasaki, Y. Shimizu and N. Koshizaki, *Small*, 2008, 2286–2291.

This journal is © The Royal Society of Chemistry 2015